Version 1.3 as of October 28, 2015

Primary author: Joel Mousseau

To be submitted to (PRL)

Comment to joelam@fnal.gov by Nov. 5th 2015

First Measurement of Partonic Nuclear Effects in Deep-Inelastic Neutrino Scattering on C, Fe and Pb at MINERvA

J. Mousseau,[1] M.Wospakrik,[1] L. Aliaga,[2,3] O. Altinok,[4] M.G. Barrios Sazo,[5] M. Betancourt,[6] A. Bodek,[7] A. Bravar,[8] H. Budd,[7] M. J. Bustamante,[3] A. Butkevich,[9] D.A. Martinez Caicedo,[10,6] M.E. Christy,[11] J. Chvojka,[7] H. da Motta,[10] M. Datta,[11] J. Devan,[2] S.A. Dytman,[12] G.A. Díaz,[3] B. Eberly,[12] J. Felix,[5] L. Fields,[13] R. Fine,[7] G.A. Fiorentini,[10] A.M. Gago,[3] H. Gallagher,[4] R. Gran,[14] D.A. Harris,[6] A. Higuera,[7,5] K. Hurtado,[10,15] T. Kafka,[4] M. Kordosky,[2] T. Le,[16,4] E. Maher,[17] S. Manly,[7] W.A. Mann,[4] C.M. Marshall,[7] K.S. McFarland,[7,6] C.L. McGivern,[12] A.M. McGowan,[7] J. Miller,[18] A. Mislivec,[7] J.G. Morfín,[6] T. Muhlbeier,[10] D. Naples,[12] J.K. Nelson,[2] A. Norrick,[2] J. Osta,[6] J.L. Palomino,[10] V. Paolone,[12] J. Park,[7] C.E. Patrick,[13] G.N. Perdue,[6,7] L. Rakotondravohitra,[6] R.D. Ransome,[16] H. Ray,[1] L. Ren,[12] P.A. Rodrigues,[7] H. Schellman,[13] D.W. Schmitz,[19,6] C. Simon,[20] J.T. Sobczyk,[6] C.J. Solano Salinas,[15] N. Tagg,[21] B.G. Tice,[16] T. Walton,[11] J. Wolcott,[7] G. Zavala,[5] and D. Zhang[2]

(MINERvA Collaboration)

[1]*University of Florida, Department of Physics, Gainesville, FL 32611*

[2]*Department of Physics, College of William & Mary, Williamsburg, Virginia 23187, USA*

[3]*Sección Física, Departamento de Ciencias, Pontificia Universidad Católica del Perú, Apartado 1761, Lima, Perú*

[4]*Physics Department, Tufts University, Medford, Massachusetts 02155, USA*

[5]*Campus León y Campus Guanajuato, Universidad de Guanajuato, Lascurain de Retana No. 5, Col. Centro. Guanajuato 36000, Guanajuato México.*

[6]*Fermi National Accelerator Laboratory, Batavia, Illinois 60510, USA*

[7]*University of Rochester, Rochester, New York 14610 USA*

[8]*University of Geneva, Geneva, Switzerland*

[9] *Institute for Nuclear Research of the Russian Academy of Sciences, 117312 Moscow, Russia*
[10] *Centro Brasileiro de Pesquisas Físicas, Rua Dr. Xavier Sigaud 150, Urca, Rio de Janeiro, RJ, 22290-180, Brazil*
[11] *Hampton University, Dept. of Physics, Hampton, Virginia 23668, USA*
[12] *Department of Physics and Astronomy, University of Pittsburgh, Pittsburgh, Pennsylvania 15260, USA*
[13] *Northwestern University, Evanston, Illinois 60208*
[14] *Department of Physics, University of Minnesota – Duluth, Duluth, Minnesota 55812, USA*
[15] *Universidad Nacional de Ingeniería, Apartado 31139, Lima, Perú*
[16] *Rutgers, The State University of New Jersey, Piscataway, New Jersey 08854, USA*
[17] *Massachusetts College of Liberal Arts, 375 Church Street, North Adams, Massachussetts 01247*
[18] *Departamento de Física, Universidad Técnica Federico Santa María, Avenida España 1680 Casilla 110-V, Valparaíso, Chile*
[19] *Enrico Fermi Institute, University of Chicago, Chicago, Illinois 60637 USA*
[20] *Department of Physics and Astronomy, University of California, Irvine, Irvine, California 92697-4575, USA*
[21] *Department of Physics, Otterbein University, 1 South Grove Street, Westerville, Ohio, 43081 USA*

(Dated: October 28, 2015)

Abstract

The MINERvA collaboration reports a novel study of neutrino + nucleus charged-current deep inelastic scattering (DIS) utilizing a neutrino beam incident on targets of hydrocarbon (scintillator), graphite, iron, and lead. Results are presented as ratios of C, Fe and Pb to CH. The ratio of the total cross sections as a function of neutrino energy and differential cross sections as a function of Bjorken-x are presented in the energy range of $5-50$ GeV. A smaller than predicted ratio of Pb / CH is measured in the nuclear shadowing region. This deficit is reflected in the DIS cross section ratio at high E_ν, and is consistent with our observations reported in a previous letter.

Deep inelastic scattering (DIS) is an important interaction for studying precision and discovery physics [1]. Starting with the confirmation of the quark parton model in the 1960s [2], high momentum transfer and high energy transfer probes have been essential in describing partonic dynamics [3]. Traditionally, these probes have been charged leptons (muons and electrons) due to the simplicity in measuring the initial and final states of the lepton.

Charged lepton DIS has been used as a partonic level tool for exploring A dependent nuclear effects on a variety of targets [4]. These effects are typically parameterized as a function of four momentum transfer squared $Q^2 = -q^2$ and the Bjorken scaling variable x [5], the fraction of the nucleon's momentum carried by the struck parton:

$$x = \frac{Q^2}{2M_N E_{had}}, \tag{1}$$

where M_N is the average nucleon mass $M_N = \frac{M_p+M_n}{2}$, and E_{had} is the energy of the final state hadrons.Four distinct effects, measured as the per nucleon ratios of absolute and differential charged lepton DIS cross sections of heavy nuclei (Fe, Au, Ca, etc. [6]) to deuterium have been identified: shadowing ($x \lesssim 0.1$, a depletion of the bound cross section [7]), anti-shadowing ($0.1 \lesssim x \lesssim 0.3$, an enhancement of the bound cross section compensating shadowing [8]), the EMC effect ($0.3 \lesssim x \lesssim 0.75$, a depletion of the bound cross-section [9] [10]) and finally Fermi motion (dominant at $x \gtrsim 0.75$, a sharp enhancement of the bound cross section [11]). While nuclear shadowing, anti-shadowing and Fermi motion are fairly well understood theoretically and experimentally, the EMC effect currently has no widely accepted theoretical origin [12].

Nuclear effects in neutrino induced DIS has been much less explored. To date no partonic nuclear effects similar to those measured for charged lepton DIS have been accurately measured due to the difficulty in combining data sets with different neutrino fluxes, acceptances, thresholds and resolutions. The analyses that do exist measure neutrino DIS off heavy nuclei such as Pb [13], and Fe[14]. Comparing the heavy nuclei measurements to free nucleon calculations in an attempt to construct neutrino nuclear effects has shown some tension with charged-lepton nuclear effects [15]. Due to these unresolved inconsistencies, the typical approach for modern neutrino DIS models has been to adapt existing charged lepton nuclear effects directly into neutrino DIS.

This letter presents a first measurement of partonic nuclear effects in charged-current DIS using the MINERvA detector. While neutrino experiments present many challenges, including knowledge of the neutrino flux and an unknown ensemble of final state interactions, neutrinos provide a unique weak-only probe of the atomic nucleus. There is no *a priori* reason to assume neutrino and charged lepton DIS will behave identically, as neutrinos are uniquely sensitive to both the axial vector and vector components of the weak nuclear force [16].

The MINERvA experiment, as well as many other current and future neutrino experiments, use the GENIE [17] event generator to simulate neutrino interactions in the detector. This generator is used to simulate the signal DIS as well as the background quasielastic, resonance and the transition region from resonant to DIS events. GENIE's simulation of DIS and transition events is based on the 2003 Bodek-Yang model [18]. The Bodek-Yang model computes cross-sections at the partonic $\nu_\mu + q$ level using GRV98NLO PDFs [19] to calculate the structure functions F_2, and xF_3. $2xF_1$ is related to F_2 via the ratio of the transverse (σ_T) to longitudinal (σ_L) cross-sections $R_L = \frac{\sigma_L}{\sigma_T}$. The R_L value used by GENIE is the Whitlow parameterization [38], and therefore:

$$2xF_1 = \frac{1 + Q^2/E_{had}}{R_L} F_2. \tag{2}$$

Bodek-Yang accounts for target mass modification and higher twist effects by calculating the nucleon structure functions as a function of a modified scaling variable ξ [18]. The ξ dependent modification made to the structure functions is currently applied identically to all elements heavier than helium. The DIS analysis presented in this letter analyzes carbon, polystyrene scintillator (CH), iron, and lead. Thus GENIE predicts identical differential and absolute DIS cross sections for these materials once acceptance, target number, and non-isoscalar effects are taken into account. We note that this treatment of the partonic nuclear effects is incomplete based on knowledge from charged lepton scattering. There is strong reason to believe shadowing must be stronger for larger nuclei [20], and the EMC effect has long known to have a strong dependence on the local nuclear density [21].

The MINERvA neutrino detector is deployed in the NuMI neutrino beam at the Fermi National Accelerator Laboratory. It is located approximately 1 km away from the neutrino production target. MINERvA uses the NuMI [22] facility as its source of neutrinos. The energy spectrum of the neutrino beam peaks at approximately 3 GeV in the NuMI low-energy configuration, with a tail which extends above 100 GeV. The generation of mesons produced from p + C collisions inside a graphite target are simulated using the GEANT [23] simulation package. External data from NA49 [24] is used to constrain and improve the pion production simulation, while MIPP thin target data [25] are used for the K/π ratio. However, the NA49 and MIPP data are only able to cover the simulation of neutrino events with an energy below 30 GeV.

The core technology of the MINERvA detector are hexagonal planes of triangular scintillator strips. These planes are used for particle tracking as well as shower reconstruction. The most upstream region of the MINERvA detector contains passive nuclear targets of solid graphite, iron, and lead each with upstream and downstream scintillator planes to provide tracking, vertexing and shower reconstruction between the targets. A liquid water target is located at the approximate midpoint of the nuclear target region, however data from the water target are not used in this analysis. The nuclear target region is followed downstream by a fully-active tracker region of scintillator planes and downstream electromagnetic and hadronic calorimeters. Each sub-detector of MINERvA is surrounded by an outer electromagnetic calorimeter as well as an outer detector consisting of steel and alternating scintillator bars used for side-exiting hadronic calorimetry. The MINERvA detector is described in detail in Ref [26]. It is located 2m upstream of the magnetized MINOS detector [27], which we use as a muon spectrometer. We require our candidate DIS interactions to contain a matched muon track in both detectors.

Charged current ν_μ DIS is characterized by a final state consisting of an outgoing μ^- and a hadronic shower with invariant mass above the resonance region. The shower consists of "hadronic energy," and is broadly defined as all deposits of energy in the detector not associated with the outgoing μ^-. All deposits of energy in the MINERvA detector are sorted into spatially associated "clusters" within each plane. Collinear clusters are used to reconstruct particle trajectories (tracks) through the passive nuclear targets, tracker, and calorimeter regions. The longest track in the recorded interaction which is matched to a track in MINOS is identified as the primary muon. MINOS-matching limits the angular acceptance of events, and muons that are within 17° of the beam direction are not included. The charge of the muon is measured via curvature in the MINOS magnetic field. The energy and momentum are measured based on the range or curvature of the muon in MINOS.

After reconstructing all available tracks, an event is assigned a vertex in the five nuclear target modules using an iterative Kalman [28] fitter when multiple tracks are available. Single track events are quite common due to reconstruction criteria and energy thresholds. As a result, approximately 20% of DIS events contain only one track in which the vertex is assigned the start point of the track. In order to fully capture single track events originating from nuclear targets, the event selection allows vertices originating in two scintillator planes downstream and one plane upstream to be included in the target sample. This leads to a background of non-nuclear target events which must be subtracted as described below.

The DIS sample is isolated using kinematic selections based on the Q^2 and invariant mass of the recoil system (W). Both quantities are calculated from the muon energy (E_μ) and outgoing muon angle (θ_μ) using:

$$Q^2 = 4E_\nu E_\mu sin^2\left(\frac{\theta_\mu}{2}\right), \quad (3)$$
$$W = \sqrt{M_N^2 + 2M_N E_{had} - Q^2},$$

where the neutrino energy is equal to the sum of the muon and hadronic energy, $E_\nu = E_\mu + E_{had}$. DIS events are required to have a $Q^2 \geq 1.0$ (GeV/c)^2 and $W \geq 2.0$ GeV/c^2. The Q^2 of these events is large enough such that the composition of the nucleon may be considered as discrete partons, and the W cut serves to remove quasielastic interactions and resonances from the sample.

The DIS measurement contains two different types of backgrounds. The first type of background stems from detector effects smearing low W and Q^2 events upward into the DIS selection. These events are estimated by normalizing the Monte Carlo (MC) simulations of the backgrounds in the passive and active targets. Two sidebands are drawn for data and simulated events in the regions 1) $Q^2 \geq 1.0$, $1.3 \leq W < 1.8$ and 2) $Q^2 < 0.8$, $W \geq 2.0$. The data in these regions are used to tune two different background templates. The first template contains all events the generator simulates with generated $W < 2.0$ (low W), and the second consists of events with a generated $W > 2.0$ and $Q^2 < 1.0$ (low Q^2). The low W template includes the quasielastic and resonant events. The normalization of each template is fit to the data simultaneously in both sidebands for each nucleus over the energy range $5.0 \leq E_\nu < 50$ GeV. The fit results are summarized in Table I. The data tend to prefer more backgrounds, especially for the low Q^2 events.

Target Material	Low W	Low Q^2
CH	0.94 ± 0.01	1.57 ± 0.02
C	0.90 ± 0.08	1.58 ± 0.11
Fe	0.99 ± 0.04	1.58 ± 0.05
Pb	0.95 ± 0.03	1.36 ± 0.05

TABLE I. Scale factors applied to the two different background templates. Low W: true $W < 2.0$ GeV/c^2. Low Q^2: true $W > 2.0$ GeV/c^2 and $Q^2 < 1.0$ (GeV/c)^2. The quoted uncertainties are statistical.

A second background arises from events mis-reconstructed in the passive nuclear target modules that actually originated in the scintillator modules surrounding the targets. Figure 1 illustrates the simulation of the CH background as well as the passive target signal. These events are subtracted by measuring the event rate of reconstructed DIS events in the MINERvA tracker modules in a manner similar to the one described in [30]. As this procedure does not fully reproduce the simulated CH background, we take the difference between the estimated and true CH background as an additional uncertainty. The nuclear target region is further away from MINOS than the fully-active region and as a result the muon acceptances are somewhat different. When using the DIS sample in the active region to estimate the CH background around the nuclear targets, we use a GEANT simulation to evaluate these acceptance corrections.

Figure 2 shows the distribution of events in data and simulation for the DIS events in iron after subtracting backgrounds and unfolding to correct detector smearing [29]. A table of such events in all nuclei may be found in the supplemental material. Our unfolding is based on Bayesian unfolding with 1 iteration, which proved to reduces biases in the unfolded distributions to the few percent level. Systematic uncertainties at the level of 20% exist primarily due to the neutrino flux. To largely cancel flux uncertainties, and to directly evaluate partonic nuclear effects, ratios of cross sections are taken between the passive targets (C, Fe, Pb) and CH. As a function of x, these ratios of the differential cross section provide direct evidence of partonic nuclear effects.

The x-differential ratios can be seen on the left of Figure 3. These ratios account for detector efficiency as well as events smearing out of the W and Q^2 cuts via an acceptance correction derived from the simulation. There is an x dependence to the ratios due to the

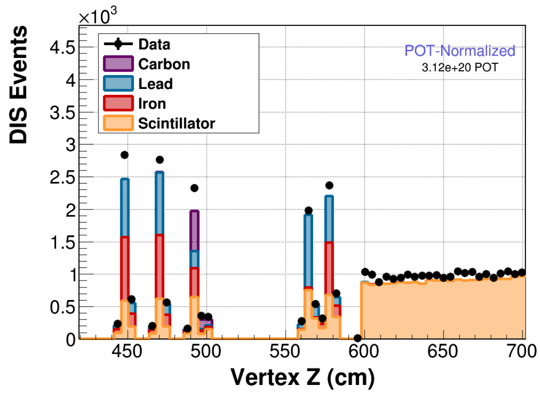

FIG. 1. The number of DIS events in the passive nuclear targets ($0 < z < 600$ cm) and tracker modules ($z > 600$ cm) as a function of longitudinal position. The orange area in the first five peaks represents the scintillator background subtracted in each nuclear target. The events located in the scintillator modules and water target between the solid targets are suppressed in this figure.

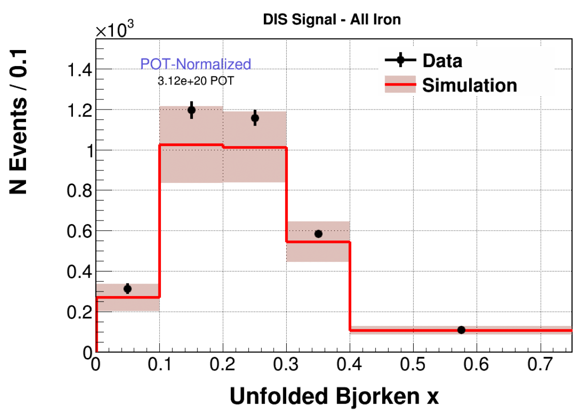

FIG. 2. Deep inelastic scattering events in iron plotted as a function of x. The total systematic error is drawn as a red band around the simulation

neutron excess in Fe and Pb. This manifests itself as an increased ratio in the valence quark region ($0.3 \leq x$) where the intermediate vector boson is predominately interacting with d quarks. Plots of the ratio corrected for these non-isoscalar effects may be found in Figure 5, included in the supplementary material. There is a possibility of a smaller than predicted Pb/CH ratio at low x. This observation could be indicative of additional nuclear shadowing in neutrino nuclear scattering. These data appear to have the same structure as in the previously published MINERvA inclusive analysis [30]: a deficit relative to the simulation at low x which increases as the size of the nucleus increases. The mean x and Q^2 of data events in that bin are approximately 0.07 and 2.0 $(\mathrm{GeV/c})^2$, respectively. The amount of shadowing observed at the average value of this bin contrasts with charged lepton scattering fits, which predict a ratio of approximately 1.0 for lead.

The ratios of carbon, iron, and lead to scintillator, display very good agreement with the simulation in the largest x bin $0.4 \leq x < 0.75$. This bin corresponds to the region where the dominant nuclear effect is the EMC effect. As GENIE simulates the EMC effect for neutrinos identically as charged leptons for all nuclei, the data imply the differences between the EMC effect in charged leptons and neutrinos must be smaller than the current MINERvA data can resolve ($\mathcal{O}(10\%)$). We note that this resolution is not sufficient to measure the EMC effect between the different nuclei, which has been shown to be $\approx 4\%$ for Pb / C [6].

The ratios of absolute cross sections as a function of E_ν for C, Fe and Pb to CH are plotted in the right side of Figure 3. Plots of the ratio corrected for the non-isoscalar effects may be found in Figure 5 included in the supplementary material. A smaller than expected ratio in the higher energy bins of the $\sigma_{\mathrm{Pb}}/\sigma_{\mathrm{CH}}$ is observed. This is consistent with the deficit in the lower x bins, as the higher energy neutrino events will tend to have a higher hadronic energy and a lower x. In contrast, the C to CH ratio at low energy is somewhat larger than unity with a large uncertainty consistent with the MC ratio of about 1.1. This is observed in the x ratios as well, where the data ratio is larger than the simulated ratios in all bins.

The data are compared with various alternative parameterizations of partonic nuclear effects applied to GENIE in Figure 4. The updated version of Bodek-Yang (BY13) [31] updates the parton distribution functions (PDFs) used in Bodek-Yang 2003 to include an A dependent parameterization of the x dependent effects based on charged lepton scattering data. This parameterization uses updated data from various experiments listed in Refs. [32] – [35]. The Cloet model consists of an independent calculation of F_2 and xF_3 based on a convolution of the Nambu-Jona-Lasinio [36] nuclear wave function with free nucleon valence PDFs [37]. The Cloet model does not include shadowing and anti-shadowing effects that dominate the $x \leq 0.3$ kinematic region. Both BY13 and Cloet have been shown to predict charged lepton DIS data in the EMC region. Our ratio calculation for the Cloet prediction assumes the Callan-Gross relationship $2xF_1 = F_2$.

While the data do not currently have the sensitivity to distinguish between the different models at higher x, we remark that the deficit in data observed in the smallest x bin cannot be explained by the updated Bodek-Yang model, the only model in the figure applicable at

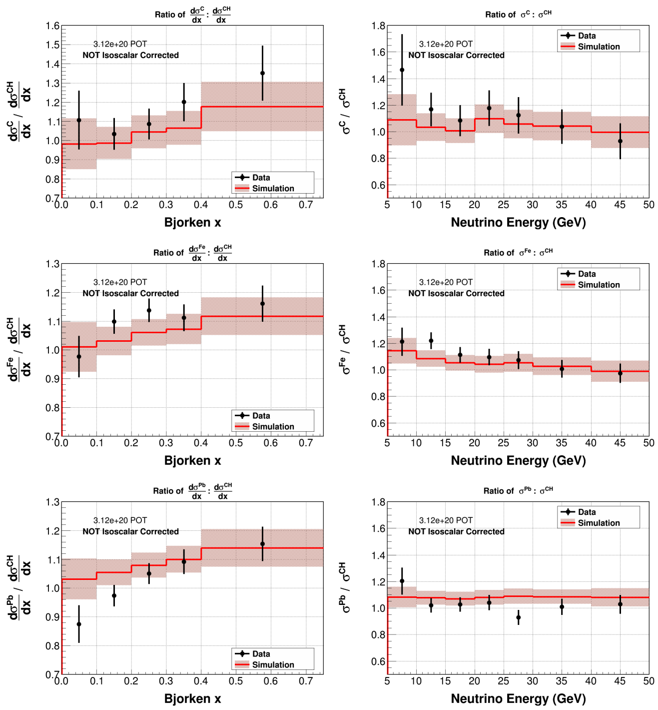

FIG. 3. Left: Ratio of the x-differential DIS cross section on C (top), Fe (center) and Pb (bottom) divided by CH. Right: Ratio of the absolute DIS cross section on C (top), Fe (center) and Pb (bottom) divided by CH as a function of E_ν. Data are drawn as points with statistical uncertainty and simulation as red lines in both cases. The total systematic error is drawn as a red band around the simulation in each histogram.

this low x. The disagreement may be explained by the fact that BY13 is a calculation based on assumptions true for charged lepton scattering, which only contains a vector current. The axial vector component of the weak current present in neutrino DIS may have a longer coherence length of the boson fluctuations responsible for nuclear shadowing [39]. This would allow shadowing to occur for neutrino scattering in the lowest x bin where vector current shadowing would be greatly suppressed. The predictions of Ref [15], based on NuTeV ν_μ -Fe and CHORUS ν_μ-Pb data are only somewhat more consistent with the data in this lowest x bin than the charged lepton-based predictions of BY13.

Neutrino-nucleus DIS presents a novel method to measure partonic nuclear effects in the weak sector. MINERvA has measured this process using a variety of nuclear targets for the first methodical measurement of neutrino nuclear effects by isolating a region of high–Q^2 and high–W events ($Q^2 \geq 1.0$ (GeV/c)^2 and $W \geq 2.0$ GeV/c^2). The measured cross section ratios show a general trend of being larger than the simulation for the lightest nucleus (C).

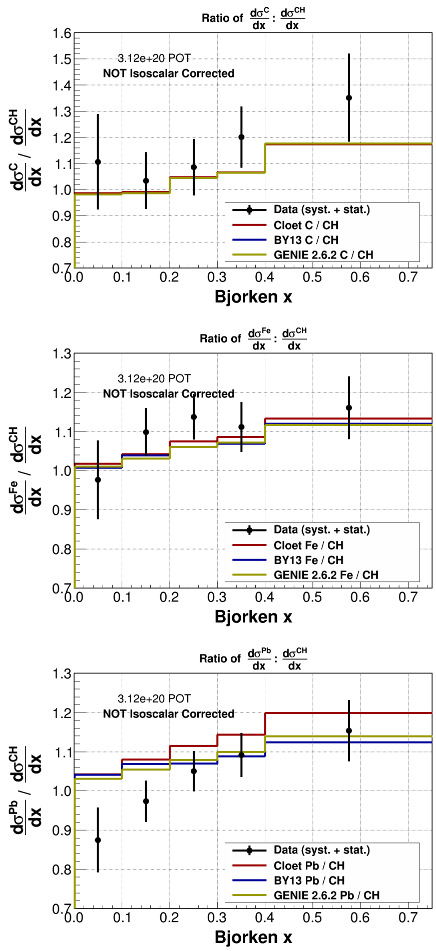

FIG. 4. DIS cross section ratios as a function of x for MINERvA data (points) and various alternative parameterizations of x dependent nuclear effects. Note that the Cloet valence quark model predictions are only valid for $x \geq 0.3$. The error bars on the data are combined statistical and systematic errors.

Conversely, the data is smaller than the simulation in the heaviest nucleus (Pb) at high energy and low x, a trend observed in a previous MINERvA analysis [30]. The data appear to agree with GENIE's treatment of the EMC effect between ($0.3 \leq x < 0.75$). The lower than expected Pb / CH ratio at large neutrino energy ($E_\nu > 20$ GeV) and low Bjorken-x ($x < 0.1$) may point to additional nuclear shadowing in the neutrino sector. Future studies with the MINERvA will posses a higher neutrino energy, and will be able to further probe this interesting shadowing region by reducing the average x of neutrino DIS events.

This work was supported by the Fermi National Accelerator Laboratory under US Department of Energy contract No. DE-AC02-07CH11359 which included the MINERvA construction project. Construction support was also granted by the United States National Science Foundation under Award PHY-0619727 and by the University of Rochester. Support for participating scientists was provided by NSF and DOE (USA), by CAPES and CNPq (Brazil), by CoNaCyT (Mexico), by CONICYT (Chile), by CONCYTEC, DGI-PUCP and IDI/IGI-UNI (Peru), by Latin American Center for Physics (CLAF), and by RAS and the Russian Ministry of Education and Science (Russia). We thank the MINOS Collaboration for use of its near detector data. We acknowledge the dedicated work of the Fermilab staff responsible for the operation and maintenance of the beamline and detector.

---

[1] J. Engelen and P. Kooijman,Prog. Part. Nucl. Phys. **41** 1-47, (1998).

[2] M. Breidenbach *et al.*, Phys. Rev. Lett. **23** (16): 935ˇ2013939 (1969).

[3] U. Landgra (NMC Collaboration) Nucl. Phys. A **527**, 123-136 (1991)

[4] D. F. Geesaman, K. Saito and A. W. Thomas, Ann. Rev. Nucl. Part. Sci. **45**, 337 (1995).

[5] J. D. Bjorken. Phys. Rev. **179**, 1547 (1969)

[6] J. Gomez *et al.* [SLAC-E139], Phys. Rev. D **49**, 4348 (1994).

[7] P. Amaudruz *et al.*, Z. Phys. **C51**, 387 (1991)

[8] J. J. Aubert *et al.* [European Muon Collaboration], Phys. Lett. B **105**, 315 (1981).

[9] J. J. Aubert, *et al.* (European Muon Collaboration), Phys. Lett. B **123**, 275 (1983).

[10] J. J. Aubert, *et al.* (European Muon Collaboration), Nucl. Phys. B **293** 740 (1987).

[11] A. Bodek and J. L. Ritchie, Phys. Rev. D **23**, 1070 (1981).

[12] I. C. Cloet, W. Bentz and A.W. Thomas *et al.* Phys. Rev. Lett. **95** 052302 (2005).

[13] Tzanov, M. *et al.* (NuTeV Collaboration) Phys. Rev. D **74** (2006).

[14] Önengüt, G. *et al.* Phys. Lett. B, **632** 1 65 - 75 (2006).

[15] K. Kovarik, *et al.*, Phys. Rev. Lett. **106** 12 (2011).

[16] Kulagin, S. A. and Petti, R. Nucl. Phys. A **765** 12 126 - 187 (2006).

[17] C. Andreopoulos *et al.*, Nucl. Instrum. Meth. **A614**, 87-104 (2010).

[18] A. Bodek, *et al.*, Nucl. Phys. Proc. Suppl. **139**, 113 (2005).

[19] A. Donnachie and P. V. Landsho, Z. Phys. C **61** 139 (1994).

[20] B. Kopeliovich and B. Povh, hep-ph/9504380.

[21] J. Arrington, A. Daniel, D. Day, N. Fomin, D. Gaskell and P. Solvignon, Phys. Rev. C **86**, 065204 (2012).

[22] P. Adamson *et al.*, arXiv:1507.06690 [physics.acc-ph].

[23] S. Agostinelli *et al.* (Geant4 collaboration) Nucl. Inst. and Meth., Phys. Res. Sect. A **506**, 250ˇ2013303 (2003).

[24] Alt, C. *et al.* (NA49 Collaboration) Eur. Phys. **49**, 897-917 (2007).

[25] J. M. Paley *et al.* (MIPP Collaboration) Phys. Rev. D **90** no. 3, 032001 (2014).

[26] L. Aliaga *et al.* (MINERvA Collaboration), Nucl. Instrum. Meth. **743C**. 130-159, (2014).

[27] D. G. Michael *et al.* (MINOS Collaboration) Nucl. Instrum. Meth. **A596**, 190-228 (2008).

[28] R. Frühwirth Nucl. Inst. and Meth. **262(2-3)**, 444-450 (1987).

[29] G. D'Agostini, Nucl. Inst .and Meth. 487-498 (1995).

[30] B. Tice *al.* (MINERvA Collaboration), Phys. Rev. Lett. **112**, 231801 (2014).

[31] A. Bodek and U. k. Yang, arXiv:1011.6592 [hep-ph].

[32] L. W. Whitlow *et al.* (SLAC-MIT), Phys. Lett. B **282** 433 (1995).

[33] A. C. Benvenuti *et al.* (BCDMS Collaboration), Phys. Lett. B **237** 592 (1990).

[34] M. Virchaux and A. Milsztajn Phys. Lett. B **274** 221 (1992).

[35] M. Arneodo et al. (NMC Collaboration), Nucl. Phys. B **483** 3 (1997).

[36] Y. Nambu and G. Jona-Lasinio Phys. Rev. **122**, 345 (1961).

[37] I. C. Cloet, Phys. Lett. **B642**, 210-217 (2006).

[38] L. W. Whitlow, *et al.*, Phys. Lett. B **250**, 193-198 (1990).

[39] B. Z. Kopeliovich *et al.* Prog. Part. Nucl. Phys. **68**, 314 (2013).

I. SUPPLEMENTAL MATERIAL

x_{bj}	I	II	III	IV	V	VI	VII	Total
0.00–0.10	13.6	2.6	6.8	3.9	4.5	4.0	3.3	17.4
0.10–0.20	7.3	4.2	3.6	1.3	3.8	1.6	1.8	10.3
0.20–0.30	6.9	3.9	3.9	2.1	3.5	2.8	1.4	10.2
0.30–0.40	8.0	0.6	5.4	3.5	3.3	1.4	1.4	11.0
0.40–0.75	11.5	5.6	8.0	3.1	3.5	1.2	1.6	15.9

TABLE II. Uncertainties as a percentage on the ratio of DIS differential cross sections $\frac{d\sigma^{C}}{dx_{bj}}/\frac{d\sigma^{CH}}{dx_{bj}}$ with respect to x_{bj} sorted by (I) data statistics, (II) CH background subtraction, (III) MC statistics, (IV) etector response to muons and hadrons (V) neutrino interactions, (VI) final state interactions, and (VII) flux and target number. The rightmost column shows the total uncertainty due to all sources.

x_{bj}	I	II	III	IV	V	VI	VII	Total
0.00–0.10	6.3	1.7	3.6	3.4	3.3	4.1	1.9	10.0
0.10–0.20	3.6	1.2	1.9	1.4	2.9	1.4	1.7	5.8
0.20–0.30	3.4	0.1	1.9	1.1	2.8	1.1	1.8	5.4
0.30–0.40	3.7	1.0	2.6	1.6	2.8	1.2	1.9	6.0
0.40–0.75	5.0	1.9	3.6	2.3	2.7	0.7	1.8	7.7

TABLE III. Uncertainties as a percentage on the ratio of DIS differential cross sections $\frac{d\sigma^{Fe}}{dx_{bj}}/\frac{d\sigma^{CH}}{dx_{bj}}$ with respect to x_{bj} sorted by (I) data statistics, (II) CH background subtraction, (III) MC statistics, (IV) etector response to muons and hadrons (V) neutrino interactions, (VI) final state interactions, and (VII) flux and target number. The rightmost column shows the total uncertainty due to all sources.

x_{bj}	I	II	III	IV	V	VI	VII	Total
0.00–0.10	5.8	1.5	3.5	2.5	2.5	2.0	2.5	8.4
0.10–0.20	3.2	1.1	1.8	0.8	2.4	1.6	1.8	5.2
0.20–0.30	3.1	0.2	1.8	0.9	2.6	1.2	1.7	5.0
0.30–0.40	3.4	0.3	2.4	1.3	2.5	0.9	1.5	5.4
0.40–0.75	4.8	1.5	3.4	1.9	3.3	1.8	1.5	7.6

TABLE IV. Uncertainties as a percentage on the ratio of DIS differential cross sections $\frac{d\sigma^{Pb}}{dx_{bj}}/\frac{d\sigma^{CH}}{dx_{bj}}$ with respect to x_{bj} sorted by (I) data statistics, (II) CH background subtraction, (III) MC statistics, (IV) etector response to muons and hadrons (V) neutrino interactions, (VI) final state interactions, and (VII) flux and target number. The rightmost column shows the total uncertainty due to all sources.

Isoscalar corrections are applied to the data and simulation to correct for the obvious difference in the per nucleon cross section of two nuclei due to the difference in the way the neutrino interacts with the bound protons and neutrons. The isoscalar correction factors out this neutron excess. Because of the lack of free nucleon cross section data for neutrino scattering, we rely on GENIE to predict the free nucleon cross sections. As MINERvA measures the ratio of cross section of different nuclei (C, Fe, Pb) to that of CH, the isoscalar correction becomes:

$$f_{\text{iso}} = \left(\frac{A}{13}\right) \frac{7\sigma(p_f) + 6\sigma(n_f)}{Z_A\sigma(p_f) + N_A\sigma(n_f)}, \tag{4}$$

where A is the atomic number, Z_A is the number of protons and N_A is the number of neutrons.

Using the GENIE predicted free nucleon cross sections and corresponding neutron and proton numbers for each nuclei in Eq. 4, we obtained the required isoscalar corrections. This correction does not take x-dependent partonic effects into account. Isoscalar corrected ratios as a function of E_ν and x may be found in Figre 5. Differences between the simulation and 1.0 in the ratios stem from under-predicted CH backgrounds which are covered by the added uncertainty.

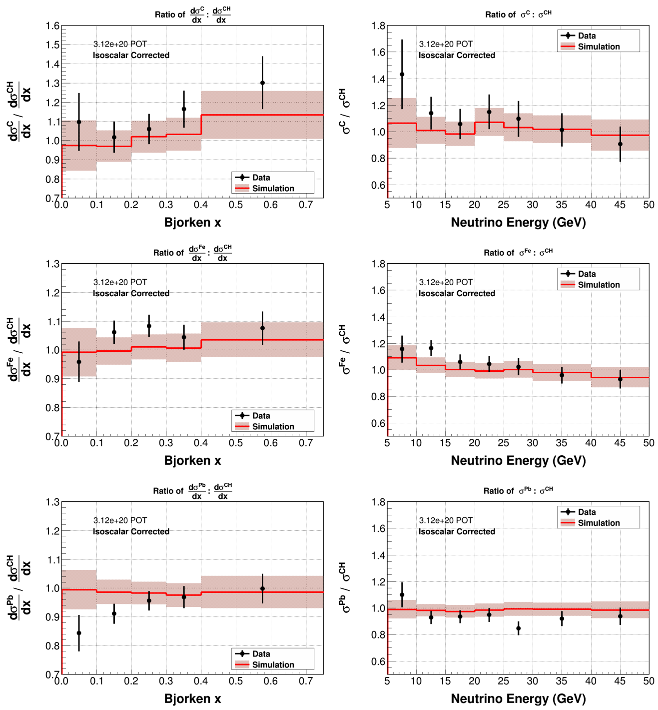

FIG. 5. Left: Isoscalar corrected ratios of the x_{bj}-differential DIS cross section on C (top), Fe (center) and Pb (bottom) divided by CH. Right: Ratio of the total DIS cross section on C (top), Fe (center) and Pb (bottom) divided by CH. Data are drawn as points with statistical uncertainty and simulation as red lines in both cases. The total systematic error is drawn as a red band around the simulation in each histogram. .

x_{bj}	C	Fe	Pb	CH
0.00–0.10	91	314	311	4789
0.10–0.20	270	1197	1222	15531
0.20–0.30	243	1158	1225	13923
0.30–0.40	139	584	689	7711
0.40–0.75	101	388	455	5020
TOTAL	846	3641	3904	47003

TABLE V. Number of DIS events in each unfolded x bin per nuclei after subtracting bacgkrounds.